Poly(lactide)/cellulose nanocrystal nanocomposites by high-shear mixing

Oguzhan Oguz, Nicolas Candau, Adrien Demongeot, Mehmet Kerem Citak, Fatma Nalan Cetin, Gregory Stoclet, Véronique Michaud, Yusuf Z. Menceloglu

Poly(lactide)/Cellulose Nanocrystal Nanocomposites by High-Shear Mixing

Oguzhan Oguz[1,2,*], Nicolas Candau[3], Adrien Demongeot[4], Mehmet Kerem Citak[1,2], Fatma Nalan Cetin[1,2], Grégory Stochlet[5], Véronique Michaud[4], Yusuf Z. Menceloglu[1,2,*]

[1]Faculty of Engineering and Natural Sciences, Materials Science and Nano Engineering, Sabanci University, 34956, Orhanli, Tuzla, Istanbul, Turkey

[2]Sabanci University Integrated Manufacturing Technologies Research and Application Center & Composite Technologies Center of Excellence, Teknopark Istanbul, 34906 Pendik, Istanbul, Turkey

[3]Centre Català del Plàstic (CCP) - Universitat Politècnica de Catalunya Barcelona Tech (EEBE-UPC), Av. D'Eduard Maristany, 16, 08019, Spain

[4]Laboratory for Processing of Advanced Composites (LPAC), Institute of Materials (IMX), École Polytechnique Fédérale de Lausanne (EPFL), Station 12, 1015, Lausanne, Switzerland

[5]Unité Matériaux Et Transformations (UMET), UMR 8207, Université de Lille, F-59000 Lille, France

**Correspondence to:*

O. Oguz; e-mail: oguzhanoguz@sabanciuniv.edu or Y. Z. Menceloglu; e-mail: yusufm@sabanciuniv.edu

ABSTRACT

There is currently considerable interest in developing stiff, strong, tough and heat resistant poly(lactide) (PLA) based materials with improved melt elasticity in response to the increasing demand for sustainable plastics. However, simultaneous optimization of stiffness, strength and toughness is a challenge for any material, and commercial PLA is well-known to be inherently brittle and temperature sensitive and to show poor melt elasticity. In this study, we report that high-shear mixing with cellulose nanocrystals (CNC) leads to significant improvements in the toughness, heat resistance and melt elasticity of PLA while further enhancing its already outstanding room temperature stiffness and strength. This is evidenced by (*i*) 1-fold increase in the elastic modulus (6.48 GPa), (*ii*) 43% increase in the tensile strength (87.1 MPa), (*iii*) 1-fold increase in the strain at break (~6%), (*iv*) 2-fold increase in the impact strength (44.2 kJ/m^2), (*v*) 113-fold increase in the storage modulus at 90 °C (787.8 MPa) and (*vi*) 10^3-fold increase in the melt elasticity at 190 °C and 1 rad/s (~10^5 Pa) via the addition of 30 wt.% CNC. It is hence possible to produce industrially viable, stiff, strong, tough and heat resistant green materials with improved melt elasticity through high-shear mixing.

Keywords: High-shear mixing, green nanocomposites, PLA, cellulose nanocrystals

1. INTRODUCTION

Biodegradable polymers[1–3] have attracted considerable interest in the plastics market in recent years as promising alternatives to petroleum based commodity polymers. However, their implementation remains a challenge because they are unable to meet the technical requirements for many components currently made from petroleum-based plastics. This is to a great extent due to their inherently poor thermal, mechanical, thermo–mechanical and/or rheological properties. Currently one of the most widely used commercial biodegradable polymers is poly(lactide) (PLA), which shows remarkable stiffness and strength,[4,5] but is intrinsically brittle and shows poor heat resistance and melt elasticity, severely limiting its range of application. Moreover, even highly stereoregular grades of PLA crystallize slowly under typical industrial processing conditions, and are highly sensitive to moisture and physical aging. Modular design strategies overcoming main limitations of PLA are therefore required to facilitate its use in commercial applications.[4–6]

PLA has also attracted attention as a matrix material for composites reinforced with various types of additive.[7,8] Cellulose-based reinforcing agents, such as micro/nano-fibers, -crystals and -whiskers, have been widely investigated for this purpose owing to their superior mechanical properties and renewable nature.[9–14] Of these, cellulose nanocrystals (CNC) are considered to be particularly effective because of their high aspect ratios.[12–14] However, their hydrophilicity renders their dispersion in hydrophobic polymers difficult and may result in interactions with the matrix that are too weak for there to be

significant reinforcement.[12–14] Over the years, a variety of techniques based, for example, on twin-screw extrusion,[15,16] solution mixing/casting,[17–19] in-situ polymerization,[20–22] low-shear melt mixing,[23] reactive functionalization and blending,[24] grafting and stereocomplexation,[25] spin coating[26] and sequential (solvent and melt) mixing[27] have been used to produce PLA-based nanocomposites reinforced with either modified or unmodified CNC, often with promising results. However, these techniques typically require precise control over multiple processing steps that include time-intensive treatments such as surface modification and an industrially viable approach capable of ensuring uniform CNC dispersion in PLA and strong PLA/CNC interactions remains elusive.

The high-shear mixing has proven to be a facile technique that allows for compounding thermoplastics with various additives even at very high filler contents (up to 80 wt.% in some cases).[28,29] Most recently, we utilized this technique to facilitate recycling of both synthetic and natural wastes by reusing them as high-added value additives to overcome main limitations of PLA.[30,31] In this regard, we produced PLA/waste cellulose microfiber composites with fiber contents up to 30 wt.% and demonstrated how much waste can be recycled by this facile technique.[30] In the meantime, we were able to show that high-shear mixing with 30 wt.% waste cellulose microfibers (WCF) resulted in notable enhancements in the elastic modulus, tensile strength and impact resistance of PLA. The elastic modulus increased from 3.1 GPa to 6.2 GPa (one-fold increase). The tensile strength increased from 60.8 MPa to 94.6 MPa (50% increase). In contrast, the strain at break decreased from 3.03% to 1.92% (37% decrease). The un-notched Charpy impact strength increased from 15.9 to 18 kJ/m^2 (20% increase). However, the highest strain at break (4.06%) and impact strength (29.7 kJ/m^2) were obtained by the addition of 5 wt.% WCF. They were, respectively 34% and 87% higher than those of pristine PLA.[30] In another study, we were able to demonstrate that this technique can also be utilized to produce super-tough polymer blends by the incorporation of waste crosslinked polyurethane (WCPU) particles into PLA as a high-added value additive.[31] The addition of 30 wt.% WCPU particles resulted in an 11-fold increase in the strain at break (~36%) and 5-fold increase in the impact strength (95 kJ/m^2) of PLA, whereas it caused to almost 50% decrease in both its elastic modulus and tensile strength. We then considered to incorporate both WCF and WCPU additives into PLA using the same technique simultaneously. This enabled us to demonstrate that it is possible to overcome main limitations of PLA, i.e. embrittlement, poor heat resistance and melt elasticity, while maintaining its outstanding stiffness and strength.[31] Consequently, our concept of utilizing the high-shear mixing for producing green materials with tunable properties while simultaneously recycling natural and synthetic wastes as high-added value additives has now been well-accepted in the literature.[30,31] However, it has not yet demonstrated whether the high-shear mixing can be utilized as an industrially viable approach capable of providing uniform dispersion of intrinsically hydrophilic high aspect ratio nanofillers in hydrophobic polymers, especially at high filler

contents. To address this issue, we have, for the first time, investigated the incorporation of 1-30 wt.% CNC into PLA via high-shear mixing without any additional treatment. We show that short mixing times (less than 1 min per 100 gram) may be sufficient to ensure uniform CNC dispersion in PLA at high filler contents and overcome the inherent embrittlement, temperature sensitivity and poor melt elasticity of PLA while further enhancing its already outstanding stiffness and strength, and hence that high-shear mixing is an effective, sustainable way of producing high performance PLA/CNC nanocomposites.

2. EXPERIMENTAL

2.1. Materials

PLA (Ingeo 4043D, $M_w \approx 150K$) was supplied by NatureWorks LLC (Minnetonka, MN). CNC was kindly provided by CelluForce (Quebec, Canada).

2.2. Nanocomposite preparation

A Gelimat G1 (Draiswerke, USA) laboratory-scale high-shear thermokinetic mixer was used to produce all the nanocomposites. The working principle and other technical details of the device were previously reported by our group.[28–32] Briefly, the blend components in particle form are accelerated by blades mounted on a high-speed shaft in a closed chamber. Part of the kinetic energy of the particles is then converted to thermal energy when they collide with the chamber wall. In the present case, the compounds were mixed at a shaft speed of 5200 rpm until the compounds temperature of 190 °C was attained. This process usually took less than one minute (≤1 min). The corresponding shear rates at the tip of the blade and at the chamber wall were estimated to be 14200 and 12060 s^{-1} respectively.[30,33,34] The resulting compound was produced in batches of 100 g without any additional processing steps and granulated at ambient temperature using a laboratory-scale granulator. The granules were then used to produce test specimens by an Xplore 12 mL laboratory-scale micro-injection molding machine that was operated at an injection temperature of 190 °C, an injection pressure of 10 bars and a mold temperature of 30 °C. Designations and compositions are given in Table 1 for all the materials investigated.

2.3. Characterization

Thermal analyses of ~10 mg specimens were carried out using a TA Q2000 Differential Scanning Calorimeter (DSC). All the results given in what follows were obtained from a first heating scan between -150 and 200 °C at a ramp rate of 10 °C/min under nitrogen. The glass transition temperature (T_g) was defined as the temperature of the inflection point of the step in heat capacity observed at around 60 °C. Equation 1 was used to calculate the degree of crystallinity, χ_{DSC};

$$\chi_{DSC} = \frac{\Delta H_m - \Delta H_{cc}}{w_f \Delta H^{\circ}_m} \times 100\% \quad (1)$$

where ΔH_m, ΔH_{cc}, w_f and ΔH°_m are respectively the enthalpy of melting, the enthalpy of cold-crystallization, the PLA

weight fraction in the nanocomposites and the latent heat of melting of 100% crystalline PLA, which is reported as 93 J/g in the literature.[35,36]

A Zeiss Gemini SEM 300 field emission scanning electron microscope (SEM) was utilized to image the tensile and impact fracture surfaces, which were coated with an ultra-thin layer of carbon.

Tensile tests were carried out according to ASTM D3039 at a cross-head speed of 2 mm/min using a Zwick Z100 Universal Testing Machine (UTM). Un-notched Charpy impact tests were performed according to ISO 179 using a CEAST Impact Tester. At least five test specimens were used in each case and all the tests were performed under ambient conditions.

A TA Q800 Dynamic Mechanical Analyzer (DMA) was used to characterize dynamic mechanical properties in single-cantilever mode using heating scans between 0 and 150 °C at a ramp rate of 3 °C/min. All the measurements were carried out in the linear viscoelastic regime with the strain amplitude of 10 μm and the frequency of 1 Hz.

Dynamic melt-rheological properties were investigated in shear mode using a TA ARES rheometer equipped with 8 mm diameter parallel-plates and frequency sweeps from 1 to 100 rad/s at 190 °C.

3. RESULTS AND DISCUSSION

3.1. Melt rheology

PLA is known to show poor melt elasticity. It is therefore difficult to produce components made from PLA using industrially relevant techniques because they typically rely on melt processing of the polymer. Hence, tailoring melt-rheological properties of PLA is important to facilitate its use in industrial applications. Figure 1 shows the effect of CNC content on the complex viscosity (η^*) and shear modulus (G') of the nanocomposites. There is an increasing trend in both η^* (Figure 1a) and G' (Figure 1b) regarding increasing CNC content. This is valid for the entire frequency range investigated and typically implies a considerable enhancement in the melt elasticity of PLA, especially at high CNC contents. On one hand, the melt elasticity of C01 is fairly similar to that of PLA. This indicates that CNC particles behave like a typical filler, which leads to an increase in the melt elasticity of PLA due to its intrinsically different elastic properties, at the filler content of 1 wt.%. On the other hand, the nanocomposites with high CNC contents, especially C20 and C30, display remarkably different melt-rheological properties in comparison to PLA. At 1 rad/s, the η^* and G' of C30 are almost three orders of magnitude higher than those of neat PLA. The difference is about two orders of magnitude at 100 rad/s. It is widely accepted that introducing a network into a polymer melt can drastically improve both η^* and G'.[31,37] We therefore attribute this remarkable enhancement in η^* and G' at the high CNC contents to the presence of the network formed by uniformly dispersed cellulose nanocrystals in PLA matrix, which will also later be shown to correspond with a change in rubbery plateau modulus as a function of CNC content.

In our previous work,[31] the incorporation of 30 wt.% waste crosslinked polyurethane (WCPU) particles resulted in a 12-fold increase in η^* and a 25-fold increase in G' of neat PLA at 1 rad/s and 190 °C. The η^* and G' at 1 rad/s were recorded as 1.07×10^4 Pa.s and 2.96×10^3 Pa, respectively. The same amount of CNC particles leads to almost three orders of magnitude increase in the η^* and G' of PLA under the same conditions (1 rad/s and 190 °C). The η^* and G' of C30 at 1 rad/s respectively are 6.87×10^5 Pa.s and 1.09×10^5 Pa. A 4-fold increase of η^* and a 5-fold increase of G' were also recorded at 100 rad/s for the polymer blend with 30 wt.% WCPU. The same concentration of CNC particles resulted in two orders of magnitude increase at 100 rad/s. The η^* and G' of C30 at 100 rad/s were recorded as 2.39×10^3 Pa.s and 1.21×10^6 Pa, respectively. As the main focus of our previous work was not to examine the effect of different cellulose based additives, we did not investigate melt-rheological properties of waste cellulose microfiber (WCF) reinforced PLA based composites. It is therefore not possible to make a comparison between CNC and WCF in terms of how they influence the melt rheological properties of PLA. However, as the main part of our previous work, we prepared some ternary blends comprising both WCPU and WCF. Of these, the composition with 15 wt.% WCPU and 15 wt% WCF displayed a η^* of 1.71×10^5 Pa.s and a G' of 1.12×10^5 at 1 rad/s. The η^* of C30 is 3-fold higher than that of this ternary blend. Their G' values, on the other hand, are almost the same. Overall, our findings strongly support the idea that high-shear mixing with various additives is an efficient way to tailor melt rheological properties of PLA. Moreover, they clearly demonstrate that CNC particles can be used as an effective rheological modifier for PLA, especially when they are uniformly incorporated at high filler contents that is possible via high-shear mixing.

3.2. CNC dispersion

A uniform dispersion of the CNC particles in the polymer matrix is of significance for the materials properties. Figure 2 shows the dispersion of CNC particles in the nanocomposite with 30 wt.% (C30), which is the highest content in this study. In general, it is very difficult to achieve a uniform CNC dispersion in a polymer matrix, even at low CNC concentrations (less than 5 wt%), due to the inherent hydrophilicity of CNC particles. To the best of our knowledge, there is no example in the literature displaying CNC dispersion in a polymer matrix at very high CNC contents on the order of 30 wt.%. We therefore do not have a reference to compare our observations regarding the CNC dispersion. However, we believe that our observations regarding CNC dispersion in PLA support the idea that high-shear mixing is an effective method for ensuring homogeneous dispersion of various additives in thermoplastics, and hence that it can be used to alter the final morphology of parent polymer. This idea was already confirmed by our previous studies various polymer blends and composites. However, with our new observations on CNC dispersion in PLA at high filler contents, it is now possible to validate that our approach can also be utilized for inherently hydrophilic fillers with very high aspect ratios to ensure uniform dispersion in a

hydrophobic matrix even at high filler concentrations. Moreover, there is another effect that was not clear in our previous works based on the same processing strategy. As shown in Figure 2, the particles are mainly aligned through the injection direction. This is attributed to the shear flow during the injection molding. This provides an indirect indication of how well the particles are integrated with the polymer matrix phase as they are not flocculated under this shear flow through the injection direction. As we considered that our claim on the uniform CNC dispersion should be supported by functional properties of the resulting nanocomposites, we also investigated their solid-state properties as elaborately discussed in the following sections.

3.3. Thermal Properties

DSC was used to examine the effect of CNC content on the thermal properties of the nanocomposites as compared to those of pure PLA. As the thermal histories of the materials are of significance for their mechanical properties, the glass transition (T_g), cold-crystallization (T_{cc}) and melting (T_m) temperatures of PLA were identified following the first heating scans (Figure 3a). The corresponding enthalpy values (areas under the cold-crystallization and melting peaks) of the first heating curves were also used to estimate the degree of PLA crystallinity (χ_{DSC}) using Eq.1 (Table 2).

There is a slight increase in the T_g and T_m values of the nanocomposites as compared to those of neat PLA. However, this is not a drastic effect. The effect of CNC content on the T_{cc}, on the other hand, is fairly substantial. It gradually increases as a function of CNC content. This indicates that CNC nanocrystals interact with amorphous PLA phase and impedes the crystallization from the glassy state. The interaction between CNC and amorphous PLA phase can also be deduced from the change in height and shape of the glass transition (Figure 3a) regarding increasing CNC content that indicates a significant decrease in the PLA chain mobility. This is also in agreement with the slightly higher T_g values recorded in the nanocomposites. Figure 3b shows that (χ_{DSC}) decreases with increasing CNC content. This implies that CNC also hinders the crystallization of PLA under the applied processing conditions. The decrease in the degree of crystallinity does not seem to be dramatic up to 10 wt.% CNC addition. However, the χ_{DSC} values of C20 and C30 are almost 45% and 60% lower than that of neat PLA. This means that the hinderance effect of CNC becomes more substantial beyond a certain concentration between 10-20% by weight. To determine this concentration, materials with CNC contents varied in between 10-20 wt.% must be produced and investigated, which is well-beyond the scope of this study.

3.4. Tensile properties

Figure 4 shows representative stress-strain curves of the materials recorded at room temperature ($T < T_g$). Accordingly, their elastic modulus (E), tensile strength (σ_{max}) and strain at break (ε_{break}) values are provided in Table 3. Just like PLA, all the nanocomposites investigated display an elastoplastic behavior comprising an evident elastic regime and yielding prior to an

apparent plastic deformation, i.e. strain softening, resulting in fracture. As a results of CNC addition, the entire stress-strain behavior of PLA is considerably altered in both elastic and plastic deformation regimes. The yielding has been proposed to be associated with the concentration of stress transmitters (ST). It is mainly governed by the nucleation and screw dislocations motion in crystalline domains.[38] The "neck width" is considered to be an indirect parameter to relate the ST concentration with the plastic deformation. Briefly, the broader neck represents the higher ST concentration. In addition, the yield stress is used as another indicator that associates the crystalline phase with the yielding.

In line with the overall stress-strain behavior of all the nanocomposites reported here, these two indicators can be used to evaluate mechanical contributions of both semi-crystalline matrix and filler phases. The neck width gradually increases with increasing CNC content up to 10 wt.% and then stays more or less constant. The yield stress, which corresponds to the tensile strength in this case, systematically increases with increasing CNC content up to 30 wt.%. This can be better explained by the fact that the cellulose nanocrystals influence the entire stress-strain both directly and indirectly. The direct effect of CNC is simply because of the fact that mechanical properties of CNC and PLA are intrinsically different than each other. CNC is a lot more elastic compared to PLA. This leads to a better elastic response, which is characterized by increasing elastic modulus with respect to increasing CNC content (Figure 5a). The indirect effect, on the other hand, is a bit more complex. At low CNC contents (1 and 5 wt.%), even though there is a slight decrease, CNC does not significantly affect the degree of crystallinity as demonstrated by the DSC analyses (Figure 3b). Hence, it is reasonable to consider that the contribution of PLA crystals is maintained. In addition, the presence of cellulose nanocrystals increases the ST concentration as they strongly interact with the matrix phase and reduces the overall PLA chain mobility, suggesting an enhanced mechanical coupling between the matrix and the filler. This also translates into an enhanced mechanical coupling between the crystalline and the amorphous phases through uniformly dispersed cellulose nanocrystals. This leads to a more effective stress distribution and hence increases both the yield strength and the extent of plastic deformation simultaneously. However, a new deformation regime begins with the addition of 10 wt.% CNC as the yield stress keeps increasing with increasing CNC content while the intensity of plastic deformation remains more or less constant. This is related to the formation of a network comprising uniformly dispersed cellulose nanocrystals that enables them to reinforce the matrix more effectively since it initiates toughening mechanisms identified by the microscopic analyses on the fracture surfaces (Figure 6 and 7). More effective reinforcement means that the cellulose nanocrystals directly contribute to both stiffening and toughening in C10, C20 and C30, whereas they provide a direct contribution to stiffening and an indirect contribution to toughening in C01 and C05.

Figure 5 shows the effect of CNC content on the E, σ_{max} and ε_{break}. Both E and σ_{max} increase with increasing CNC content

(Figure 5a and 5b). The ε_{break}, on the other hand, increases with increasing CNC content up to 10 wt.% and then remains more or less constant. The *E* values of C01, C05, C10, C20 and C30 are about 13, 29, 62, 85 and 110% higher than that of the neat PLA, respectively. C30 displays the maximum value of *E* recorded as 6.48 GPa. Moreover, the incorporation of CNC into PLA matrix resulted in a notable enhancement in its σ_{max}, which is increased by almost 5, 14, 20, 31 and 43% in C01, C05, C10, C20 and C30, respectively. C30 shows the highest σ_{max} value noted as 87.1 MPa. The ε_{break} values of C01 and C05 are approximately 42 and 69% higher than that of the neat PLA. C10, C20 and C30 display more or less the same ε_{break} on the order of 6% that is almost 1-fold higher as compared to that of the neat PLA.

Typical CNC contents in PLA/CNC nanocomposites reported in the literature are usually less than 10 wt.%. Hence, it is not easy to directly compare our results with the results obtained from PLA/CNC nanocomposites. However, it is possible to compare them with the results obtained from PLA based composites reinforced by different forms of cellulose at similar filler contents.[7,10,13,14,39,40] For example, Mathew et. al.[39] used extrusion and injection molding to produce unmodified microcrystalline cellulose (MCC) filled PLA based composites. As a result of 25 wt.% MCC loading, a 40% increase was observed in the *E* of neat PLA but its σ_{max} decreased from 49.6 MPa to 36.2 MPa. In another study, [40] an *E* of 5.8 GPa and a σ_{max} of 92 MPa were obtained by loading 30 wt.% synthetic cellulose fibers into PLA via a combined molding approach comprising two-step extrusion coating process and subsequent injection molding. A considerable increase in the *E* via the addition of cellulose based fillers are well-known in the literature but the σ_{max} strongly depends on the filler type, processing conditions, filler distribution and polymer-filler interactions.[10,13,30,31,39,40,41] Both *E* and σ_{max} values of our materials are either higher or comparable than those of cellulose reinforced PLA based composites. The notable improvements in the *E* and σ_{max} of PLA in our case are originated from the fact that the high-shear mixing favours the uniform distribution of CNC and hence that enables the matrix and the filler phases to strongly interact with each other. This allows the applied stress to be trasmitted from one to the other efficiently, leading to drastically stiffness and strength at the same time. This idea may be supported by examining, for example, the non-linear change in the σ_{max} regarding CNC concentration (Figure 5b) indicating a threshold that may become apparent at CNC contents higher than 30 wt.%. This kind of change has reported in the literature for PLA/fiber composite systems.[41] The gradual increase in the σ_{max} implies a decrease in the reinforcing effect of CNC with respect to the increase in its concentration. For example, the addition of 10 wt.% CNC resulted in an almost 13 MPa enhancement in the strength, but only an increase of about 6 MPa was recorded when the CNC content was increased from 10 to 20 wt.%. A possible explanation is that cellulose nanocrystals inevitably begin to interact with each other beyond a certain concentration. However, in such cases, final materials are usually not able to maintain the plastic deformation due to filler dominated stress-strain behavior.[30] In contrast, all the nanocomposites investigated here,

including those with very high filler contents (C20 and C30), maintain the plastic deformation although the probability of filler interactions is fairly high. It is therefore reasonable to consider that there is a network formed by uniformly dispersed cellulose nanocrystals that enables them to work with the stress transmitters cooperatively and avoid a probable catastrophic failure effect of filler-filler interactions through various energy dissipation, i.e. toughening, mechanisms (Figure 7), which will be discussed later. However, it is clear that even the nanocomposites with very high CNC contents maintain the plastic deformation as demonstrated by the strain at break values. Nevertheless, it is worth to note that the trend in the ε_{break} is somewhat unusual as compared to those reported for cellulose reinforced PLA based composites in the literature. To the best of our knowledge, the ε_{break} in such composites with similar filler contents in the range of 10-40 wt.% typically decreases with increasing filler content.[9,30,42]

Figure 6 displays SEM images of the tensile-fracture surfaces of PLA, C01 and C30. PLA shows typical deformation marks[30] representing both brittle and ductile fracture modes, such as random bumps and voids (brittle failure mode) and wavy streamlines (ductile failure mode) (Figure 6a).

The addition of CNC drastically changes this typical fracture pattern. Even with the addition of only 1 wt.% CNC, the fracture surface of the material (Figure 6b) is largely covered by the plastic deformation marks. They are mainly formed by shear yielding following debonding at the polymer-filler interfaces as a result of an increment in the stress concentration due to the presence of CNC fillers. This increment is because elastic properties of the matrix and the filler are significantly different than each other. This intrinsic difference accumulates the stress around the CNC particles, which then leads to debonding at the polymer-filler interfaces, and hence the void formation tailoring the stress state in the polymer phase surrounding the voids. This then initiates the volumetric strain release and hence the shear yielding dissipating considerable amount of energy upon deformation. The materials that this mechanism takes place often show large plastic deformation through crack propagation. Details regarding this mechanism are reported elsewhere.[43,44] The nature of this mechanism provides a clear-cut evidence for our claim that the CNC fillers directly contributes to stiffening while providing an indirect contribution to toughening in C01 and C05. Figure 6c displays the fracture surface of C30 that is a lot more complex, and more importantly, significantly different than those of PLA and C01. This is mainly due to the presence of various key deformation mechanisms that provides a strong support for our claim that the CNC fillers directly contributes to both stiffening and toughening in the materials with high CNC contents. Figure 7 shows the deformation marks representing these key deformation mechanisms that can be listed as shear yielding,[4,30,31,49,50] (Figure 7a-e), which follows debonding at the polymer-filler interface,[30] multiple crazing[4,30,31] (Figure 7a and 7b), plastic void growth[31, 45–47] (Figure 7a-e), fibrillation[31,48] (Figure 7a-e) and nano-cavitation[31,45] (Figure 7f). These mechanisms cooperatively act along the multiple

length scales and allow for simultaneous stiffening, strengthening and toughening and hence a remarkable damage tolerance.

3.5. Impact properties

The effect of CNC content on the room temperature (unnotched Charpy) impact properties of PLA and PLA/CNC is shown in Figure 8. The data from the impact tests are provided in Table 3. The impact strength of PLA increases with increasing CNC content and then reaches to the maximum value of 44.2 kJ/m^2. This change is similar to that of the strain at break. The impact strength values of C01, C05, C10, C20 and C30 are about 48, 93, 136, 156 and 178% higher than that of PLA. The deformation mechanisms highlighted in the previous section also act upon impact deformation. Figure 9 shows the SEM images of the impact-fracture surfaces of PLA, C01 and C30.

The yellow arrows on the micrographs indicate the impact direction. PLA shows a very smooth fracture surface representing the brittle fracture (Figure 9a), whereas the fracture surface of C1 (Figure 9b) is rough and fully covered by wavy streamlines and looks like the surface of a “choppy sea” that typically represents an intensive plastic deformation occurred in ductile failure because of shear yielding. The fracture surface of C30 (Figure 9c), on the other hand, is highly rough and complex and comprises various toughening mechanisms indicated by the deformation marks highlighted in Figure 10. They can be summarized as plastic void growth[31, 45–47] (Figure 10a-c), multiple crazing[4,30,31] (Figure 10a, 10c and 10d), fibrillation[31,48] (Figure 10a and 10c), nano-cavitation[31,45] (Figure 10b and 10c), the formation of dimples[31] (Figure 10d) and *fold-thrust belt* like layered structures[31] (Figure 10a, 10b, 10e and 10f) following a sudden increase in stress concentration leading to debonding at polymer-filler interface and an extensive shear yielding.

3.6. Dynamic mechanical properties

Figure 11a and 11b display storage modulus (E') and loss factor ($tan\ \delta$) of the materials as a function of temperature. Quantitative results obtained from DMA measurements are listed in Table 4. Just like the neat PLA, C01 and C05 display a sharp drop in E' (Figure 11a) and thus a sharp peak in $tan\ \delta$ (Figure 11b) centred around 75 °C and then an increment in E' after a plateau. The former is associated with α-relaxation of the matrix phase, whereas the latter is related to its cold-crystallization. C10, C20 and C30, on the other hand, show a notably different behavior. The α-relaxation temperature (T_α) was determined by three different methods that can be listed as (*i*) T_α by E' onset, (*ii*) T_α by E'' peak and (*iii*) T_α by $tan\ \delta$ peak, respectively.[31]

The quantitative values of these three parameters (Table 4) are not significantly affected by the incorporation of CNC. However, the effect of CNC on the α-relaxation is much more apparent in both magnitude and shape of the transition as observed in both E' and $tan\ \delta$ curves (Figure 11a and 11b). The magnitude of the transition, i.e. both the drop in E' and the

tan δ peak, decrease with increasing CNC content that also leads to an increasingly broader transition. These results are in a good agreement with the DSC results and mainly suggest that the α-relaxation of mobile amorphous PLA phase significantly slows down with increasing CNC content, indicating a greatly hindered chain mobility due to the immobilization of mobile amorphous PLA phase at the PLA-CNC interfaces as a result of the strong interactions between amorphous PLA phase and CNC. In addition, the cold-crystallization behavior is also significantly affected by the incorporation of 10, 20 and 30 wt.% CNC. While C10 still shows a slight increase in E' after the rubbery plateau, C20 and C30 do not display this behavior. This indicates that the cold-crystallization of PLA still takes place in C10, but is completely hindered in C20 and C30. This is also in agreement with the DSC results, suggesting that CNC impedes the PLA crystallization from the glassy state.

One of the main limitations of PLA is its low heat resistance, which is due to the sharp drop in elastic properties after the glass transition temperature. This is typically characterized by the E' at 90 °C, which represents the rubbery plateau modulus.[31] To evaluate whether the incorporation of CNC into PLA has an effect on its heat resistance or not, the E' at 90 °C values are plotted against CNC concentration (Figure 11c). There is a considerable increase in the rubbery plateau modulus regarding the increase in CNC concentration. This strongly suggests a remarkable enhancement in the heat resistance. The E' at 90 °C values of C01, C05, C10, C20 and C30, respectively, are 1.3, 3.1, 28, 77 and 113-times higher as compared to that of pristine PLA. The change in the rubbery plateau modulus is attributed to the network of well-dispersed cellulose nanocrystals in PLA matrix. Overall, DMA results clearly suggest that dynamic mechanical properties of PLA as well as its heat resistance can be significantly tailored by the addition of CNC.

4. CONCLUSION

Stiff, strong and tough cellulose nanocrystal reinforced poly(lactic) acid based nanocomposites with enhanced heat resistance and melt elasticity were successfully produced by high-shear thermokinetic mixing. This approach offers an effective way to produce high performance nanocomposites as it is based on the use of a facile technique ensuring uniform filler dispersion even at very high filler contents.

Achieving the uniform dispersion of CNC in a polymer matrix is a challenge. Here we demonstrate that the high-shear mixing in short time scales may be sufficient to overcome this challenge. This is possible without any time-intensive pre-treatment even at filler contents as high as 30 wt.%.

Main limitations of PLA are often listed as inherent embrittlement, high temperature sensitivity and poor melt elasticity. Our results clearly demonstrate that incorporation of CNC into PLA via high-shear mixing can overcome these limitations while further enhancing already remarkable room temperature stiffness and strength of PLA. This is evidenced by (*i*) 1-fold

increase in the elastic modulus, (*ii*) 43% increase in the tensile strength, (*iii*) 1-fold increase in the strain at break, (*iv*) 2-fold increase in the impact strength at 25 °C and (*v*) considerable enhancements in the heat resistance and melt elasticity characterized by approximately $\sim 10^2$ increase in the E' at 90 °C and $\sim 10^3$ increase in the η^* and G' at 190 °C and 1 rad/s. The technique demonstrated here can be scaled up. Hence, it provides an industrially viable option for the mass production of sustainable plastics with tunable materials property profiles.

ACKNOWLEDGMENTS

We sincerely thank CelluForce for kindly providing the CNC.

ORCID

Oguzhan Oguz: 0000-0002-4457-5274

Yusuf Z. Menceloglu: 0000-0003-0296-827X

NOTES

The authors declare no competing financial interest.

REFERENCES

[1] R.A. Gross, B. Kalra, *Science* **2002**, *297*, 803.

[2] S. Agarwal, *Macromol. Chem. Phys.* **2020**, *221*, 2000017.

[3] S. RameshKumar, P. Shaiju, K.E. O'Connor, P. R. Babu, *Curr. Opin. Green Sustain. Chem.* **2020**, *21*, 75.

[4] V. Nagarajan, A.K. Mohanty, M. Misra, *ACS Sustainable Chem. Eng.* **2016**, *4*, 2899.

[5] V. Nagarajan, K. Zhang, M. Misra, A.K. Mohanty, *ACS Appl. Mater. Interfaces* **2015**, *7*, 11203.

[6] L.-T. Lim, R. Auras, M. Rubino, *Prog. Polym. Sci.* **2008**, *33*, 820.

[7] J.-M. Raquez, Y. Habibi, M. Murariu, P. Dubois, *Prog. Polym. Sci.* **2013**, *38*, 1504.

[8] M. Murariu, P. Dubois, *Adv. Drug Deliv. Rev.* **2016**, *107*, 17.

[9] K. Oksman, M. Skrifvars, J.-F. Selin, *Compos. Sci. Technol.* **2003**, *63*, 1317.

[10] O. Faruk, A.K. Bledzki, H.-P. Fink, M. Sain, *Prog. Polym. Sci.* **2012**, *37*, 1552.

[11] J. Cailloux, J.M. Raquez, G.L. Re, O. Santana, L. Bonnaud, P. Dubois, M.L. Maspoch, *Carbohydr. Polym.* **2019**, *224*, 115188.

[12] C. Calvino, N. Macke, R. Kato, S.J. Rowan, *Prog. Polym. Sci.* **2020**, *103*, 101221.

[13] F.V. Ferreira, A. Dufresne, I.F. Pinheiro, D.H.S. Souza, R.F. Gouveia, L.H.I. Mei, L.M.F. Lona, *Eur. Polym. J.* **2018**, *108*, 274.

[14] M. Mariano, N.E. Kissi, A. Dufresne, *J. Polym. Sci., Part A: Polym. Phys.* **2014**, *52*, 791.

[15] E.M. Sullivan, R.J. Moon, K. Kalaitzidou, *Materials* **2015**, *8*, 8106.

[16] S.H. Sung, Y. Chang, J. Han, *Carbohydr. Polym.* **2017**, *169*, 495.

[17] D. Bagheriasl, P.J. Carreau, B. Riedl, C. Dubois, W.Y. Hamad, *Cellulose* **2016**, *23*, 1885.

[18] E. Fortunati, F. Luzi, D. Puglia, R. Petrucci, J.M. Kenny, L. Torre, *Ind. Crops Prod.* **2015**, *67*, 439.

[19] N. Lin, J. Huang, P.R. Chang, J. Feng, J. Yu, *Carbohydr. Polym.* **2011**, *83*, 1834.

[20] H. Chai, Y. Chang, Y. Zhang, Z. Chen, Y. Zhong, L. Zhang, X. Sui, H. Xu, Z. Mao, *Int. J. Biol. Macromol.* **2020**, *155*, 1578.

[21] S. Gazzotti, H. Farina, G. Lesma, R. Rampazzo, L. Piergiovanni, M.A. Ortenzi, A. Silvani, *Eur. Polym. J.* **2017**, *94*, 173.

[22] C. Miao, W.Y. Hamad, *Carbohydr. Polym.* **2016**, *153*, 549.

[23] M.R. Kamal, V. Khoshkava, *Carbohydr. Polym.* **2015**, *123*, 105.

[24] M. Pracella, Md.M.-U. Haque, D. Puglia, *Polymer* **2014**, *55*, 3720.

[25] J.K. Muiruri, S. Liu, W.S. Teo, J. Kong, C. He, *ACS Sustainable Chem. Eng.* **2017**, *5*, 3929.

[26] J. Shojaeiarani, D.S. Bajwa, N.M. Stark, S.G. Bajwa, *Composites, Part B* **2019**, *161*, 483.

[27] A. Arias, M.-C. Heuzey, M.A. Huneault, G. Ausias, A. Bendahou, *Cellulose* **2015**, *22*, 483.

[28] O. Oguz, E. Simsek, K. Bilge, Y.Z. Menceloglu, *Int. Polym. Process.* **2017**, *32*, 562.

[29] E. Simsek, O. Oguz, K. Bilge, M.K. Citak, O. Colak, Y.Z. Menceloglu, *J. Elastomers Plast.* **2018**, *50*, 537.

[30] O. Oguz, K. Bilge, E. Simsek, M.K. Citak, A.A. Wis, G. Ozkoc, Y.Z. Menceloglu, *Ind. Eng. Chem. Res.* **2017**, *56*, 8568.

[31] O. Oguz, N. Candau, M.K. Citak, F.N. Cetin, S. Avaz Seven, Y.Z. Menceloglu, *ACS Sustainable Chem. Eng.* **2019**, *7*, 7869.

[32] İ. Özen, F. İnceoğlu, K. Acatay, Y.Z. Menceloğlu, *Polym. Eng. Sci.* **2012**, *52*, 1537.

[33] T.G. Gopakumar, D.J.Y.S. Pagé, *J. Appl. Polym. Sci* **2005**, *96*, 1557.

[34] T.G. Gopakumar, D.J.Y.S. Pagé, *Polym. Eng. Sci.* **2004**, *44*, 1162.

[35] A. Magoń, M. Pyda, *Polymer* **2009**, *50*, 3967.

[36] M.C. Righetti, E. Tombari, *Thermochim. Acta* **2011**, *522*, 118.

[37] Y.-S. He, J.-B. Zeng, G.-C. Liu, Q.-T. Li, Y.-Z. Wang, *RSC Adv.* **2014**, *4*, 12857.

[38] S. Humbert, O. Lame, G. Vigier, *Polymer* **2009**, *50*, 3755.

[39] A.P. Mathew, K. Oksman, M. Sain, *J. Appl. Polym. Sci.* **2005**, 97, 2014.

[40] A.K. Bledzki, A. Jaszkiewicz, D. Scherzer, *Composites, Part A* **2009**, 40, 404.

[41] M.A. Sawpan, K.L. Pickering, A. Fernyhough, *Composites, Part A* **2011**, *42*, 310.

[42] M. Jonoobi, J. Harun, A.P. Mathew, K. Oksman, *Compos. Sci. Technol.* **2010**, *70*, 1742.

[43] W.C.J. Zuiderduin, J. Huétink, R.J. Gaymans, *Polymer* **2006**, *47*, 5880.

[44] W.C.J. Zuiderduin, C. Westzaan, J. Huétink, R.J. Gaymans, *Polymer* **2003**, *44*, 261.

[45] B.T. Marouf, Y.-W. Mai, R. Bagheri, R.A. Pearson, *Polym. Rev.***2016**, *56*, 70.

[46] B.B. Johnsen, A.J. Kinloch, R.D. Mohammed, A.C. Taylor, S. Sprenger, *Polymer* **2007**, *48*, 530.

[47] J.G. Williams, *Compos. Sci. Technol.* **2010**, *70*, 885.

[48] B. Na, W. Xu, R. Lv, Z. Li, N. Tian, S. Zou, *Macromolecules* **2010**, *43*, 3911.

[49] H. Liu, J. Zhang, *J. Polym. Sci., Part A: Polym. Phys.* **2011**, *49*, 1051.

[50] G. Kfoury, J.-M. Raquez, F. Hassouna, J. Odent, V. Toniazzo, D. Ruch, P. Dubois, *Front. Chem.* **2013**, *1*.

LIST OF FIGURES

Figure 11. Dynamic mechanical properties of pure PLA and PLA/CNC nanocomposites; (a) *E′* vs. *T* and (b) *tan d* vs. *T* and (c) *E′* at 90 °C vs. CNC content.

Each figure is uploaded as a separate file.

LIST OF TABLES

Table 1: Specimen designations and compositions.

Table 2. Thermal properties of all the materials investigated.

Table 3. Mechanical properties of neat PLA and PLA/CNC nanocomposites.

Table 4. Dynamic mechanical properties of neat PLA and PLA/CNC nanocomposites.

Each table is uploaded as a separate file.

TOC GRAPHIC / *For Table of Contents use only*

The TOC graphic is uploaded as a separate file.

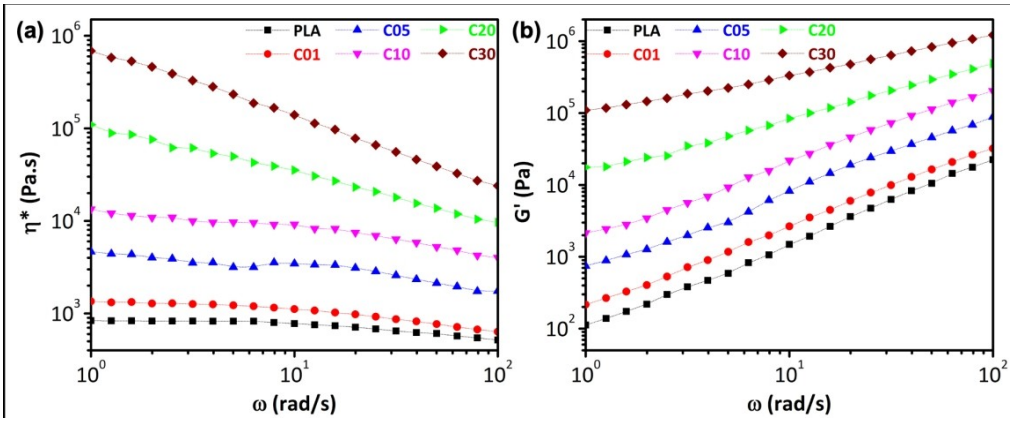

Figure 1. The effect of CNC content on the complex viscosity (η^*) and shear modulus (G') of the materials in the frequency (ω) range of 1–100 rad/s.

40x16mm (1200 x 1200 DPI)

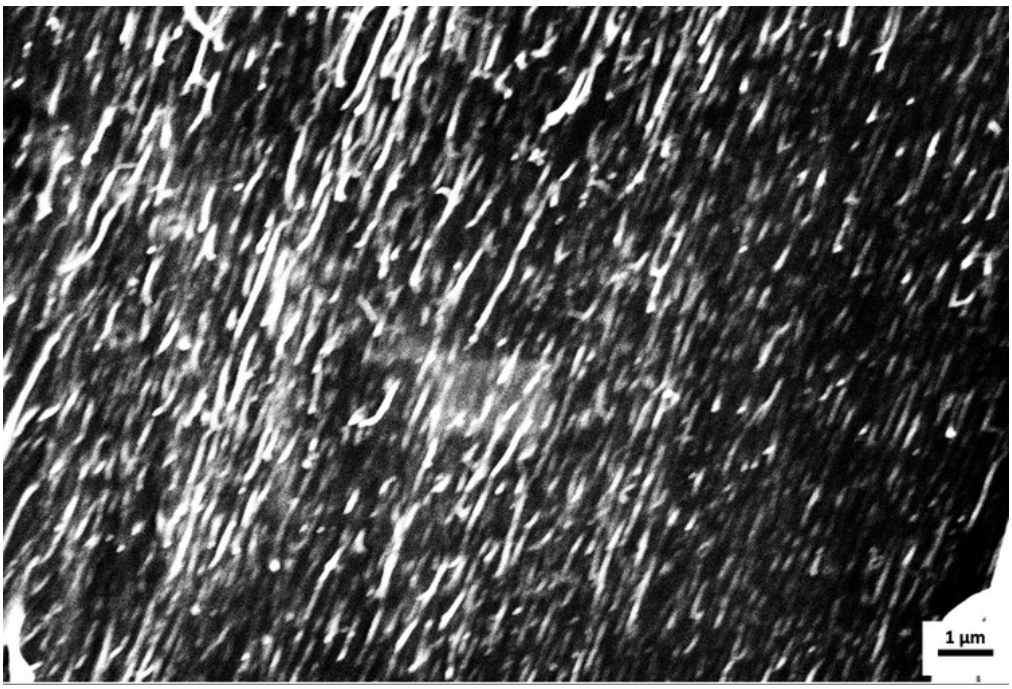

Figure 2. The SEM observation on the cross-section of C30 displaying the dispersion of CNC particles recorded by an in-lens detector.

31x21mm (600 x 600 DPI)

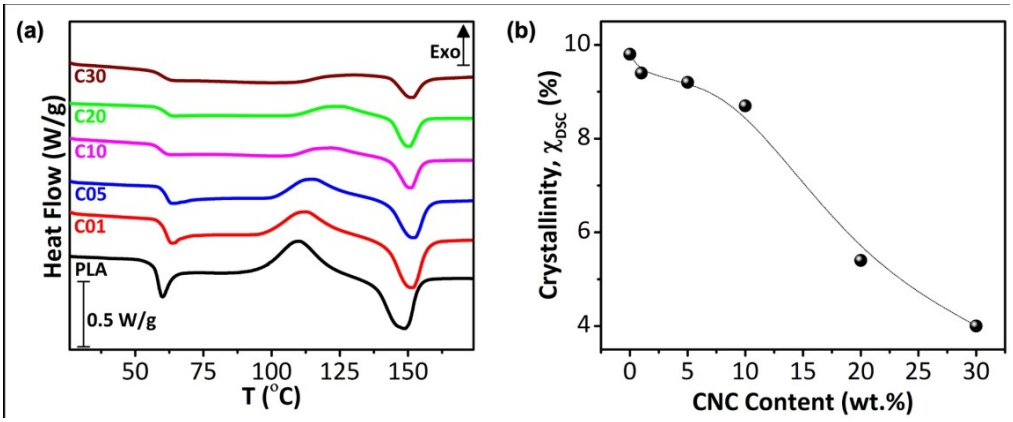

Figure 3. (a) The first heating DSC scans of all the materials investigated and (b) the change in the χ_{DSC} as a function of CNC content.

54x22mm (1200 x 1200 DPI)

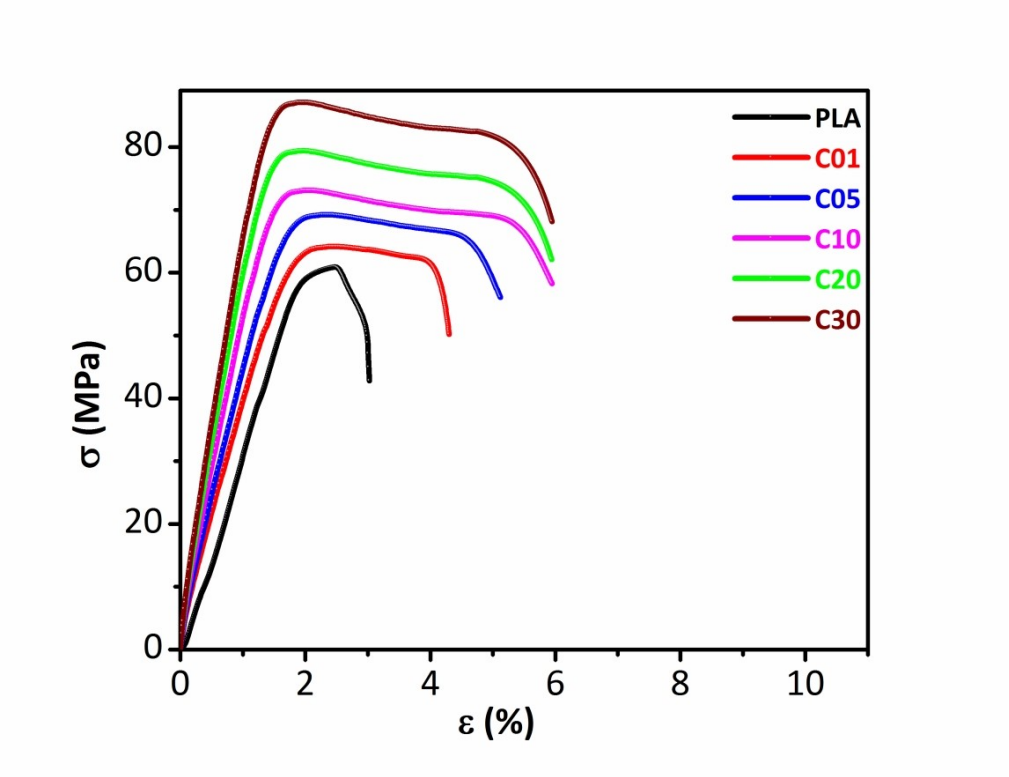

Figure 4. Stress-strain behavior of all the materials investigated.

69x53mm (1200 x 1200 DPI)

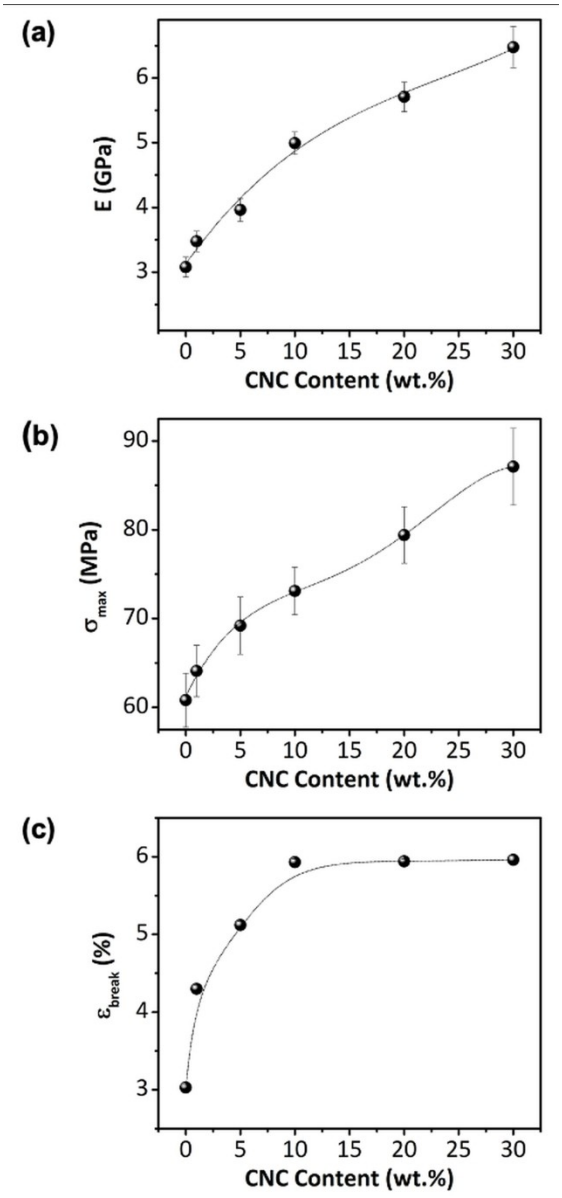

Figure 5. Tensile properties of pure PLA and PLA/CNC nanocomposites; (a) E, (b) σ_{max} and (c) ε_{break} as a function of CNC content.

54x116mm (1200 x 1200 DPI)

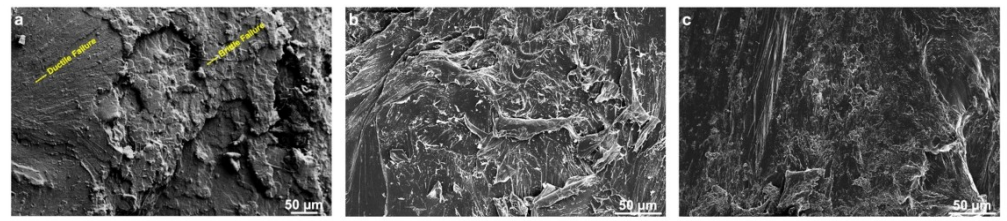

Figure 6. Low-magnification SEM images of the tensile-fracture surfaces: (a) PLA, (b) C01 and (c) C30.

54x13mm (1200 x 1200 DPI)

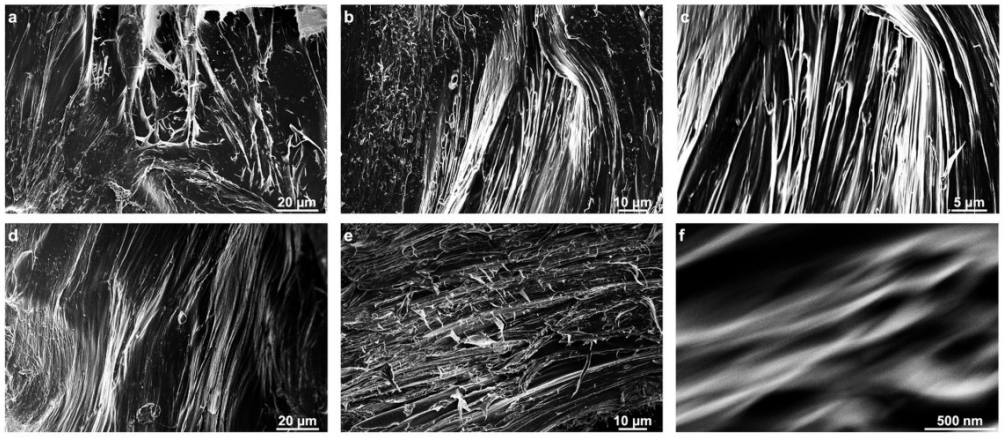

Figure 7. High-magnification SEM images displaying deformation marks on the tensile-fracture surface of C30 associated with (a-e) shear yielding, (a, b) multiple crazing, (a-e) plastic void growth, (a-e) fibrillation and (f) nano-cavitation.

54x24mm (1200 x 1200 DPI)

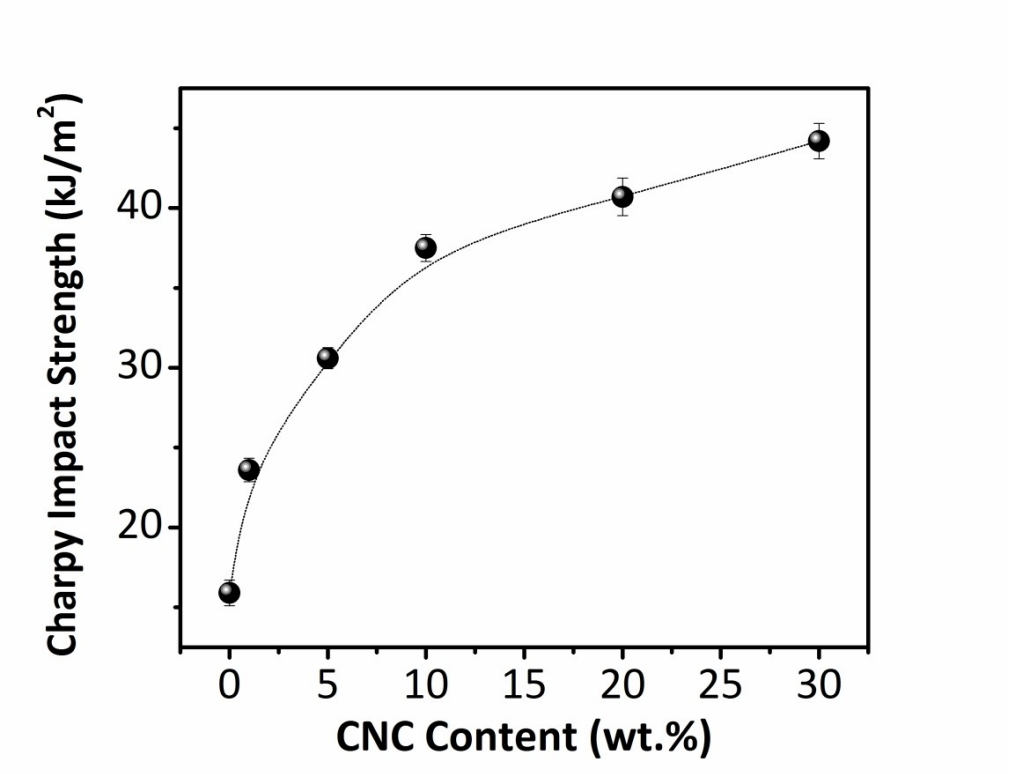

Figure 8. The un-notched Charpy impact strength vs. CNC content (wt.%).

69x53mm (1200 x 1200 DPI)

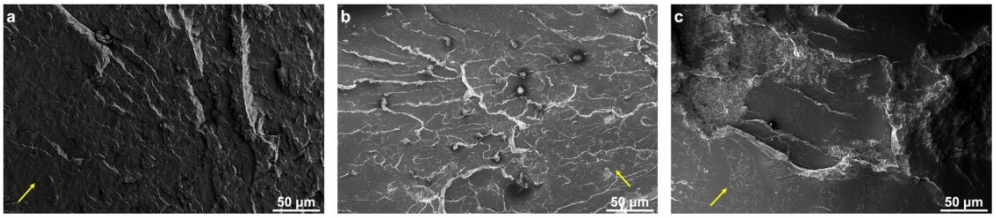

Figure 9. SEM images of the impact-fracture surfaces of (a) PLA, (b) C01 and (c) C30.

54x13mm (1200 x 1200 DPI)

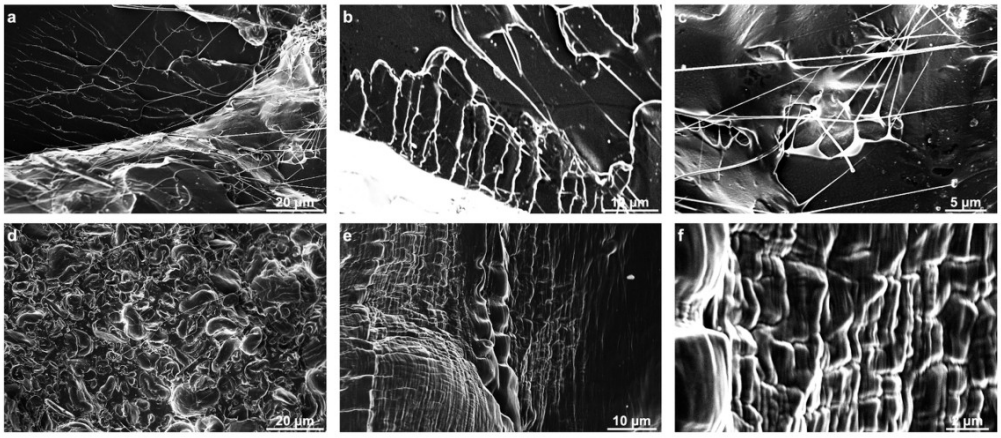

Figure 10. SEM images showing deformation marks on the impact-fracture surface of C30 related to (a, b, c) plastic void growth, (a, c, d) multiple crazing, (a, c) fibrillation, (b, c) nano-cavitation and the formation of (d) dimples and (a, b, e, f) fold-thrust belt like layered structures.

54x24mm (1200 x 1200 DPI)

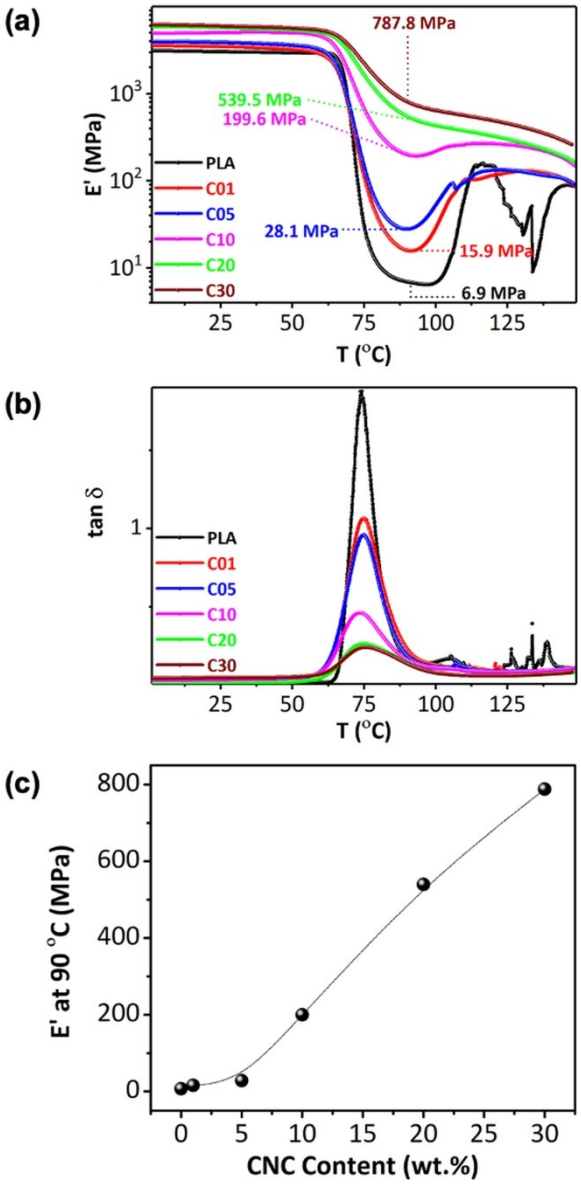

Figure 11. Dynamic mechanical properties of pure PLA and PLA/CNC nanocomposites; (a) *E´* vs. *T* and (b) *tan δ* vs. *T* and (c) *E´* at 90 °C vs. CNC content.

54x106mm (1200 x 1200 DPI)

Table 1: Specimen designations and compositions.

Specimen Designation	PLA Content (wt.%)	CNC Content (wt.%)
PLA	100	0
C01	99	1
C05	95	5
C10	90	10
C20	80	20
C30	70	30

Table 2. Thermal properties of all the materials investigated.

Specimen	T_g (°C)	T_{cc} (°C)	ΔH_{cc} (J/g)	T_m (°C)	ΔH_m (J/g)	$\chi_{DSC}(\%)$
PLA	58.1±1	109.8	17.72	149.0	26.81	9.8
C01	61.5±1	111.2	15.62	151.4	24.23	9.4
C05	61.8±1	113.6	15.33	152.1	23.41	9.2
C10	58.9±1	121.9	9.80	150.7	17.10	8.7
C20	61.4±1	125.1	9.11	150.0	13.14	5.4
C30	60.2±1	127.6	4.09	151.4	6.71	4.0

Table 3. Mechanical properties of neat PLA and PLA/CNC nanocomposites.

Sample	E (MPa)	σ_{max} (MPa)	ε_{break} (%)	*Unnotched Charpy Impact Strength* (kJ/m^2)
PLA	3079±154	60.8±3.04	3.03±0.03	15.9±0.80
C01	3476±159	64.1±2.89	4.30±0.05	23.6±0.73
C05	3963±177	69.2±3.22	5.12±0.05	30.6±0.66
C10	4992±173	73.1±2.68	5.93±0.04	37.5±0.84
C20	5708±230	79.4±3.18	5.94±0.03	40.7±1.17
C30	6476±319	87.1±4.32	5.96±0.06	44.2±1.11

Table 4. Dynamic mechanical properties of neat PLA and PLA/CNC nanocomposites.

Sample	*E' at 25 °C* (MPa)	*E' at 90 °C* (MPa)	$^{PLA}T_{\alpha}$ *by E' onset* (°C)	$^{PLA}T_{\alpha}$ *by E'' peak* (°C)	$^{PLA}T_{\alpha}$ *by tan δ peak* (°C)
PLA	3053±177	6.9±0.4	67.8±1	68.7±1	74.2±1
C01	3500±132	15.9±0.6	65.1±1	67.3±1	74.8±1
C05	3898±153	28.1±1.1	64.7±1	66.9±1	75.0±1
C10	5060±142	199.6±5.6	63.9±1	67.3±1	73.4±1
C20	5755±100	539.5±9.4	65.1±1	69.4±1	74.7±1
C30	6564±173	787.7±20.8	65.6±1	70.1±1	75.6±1

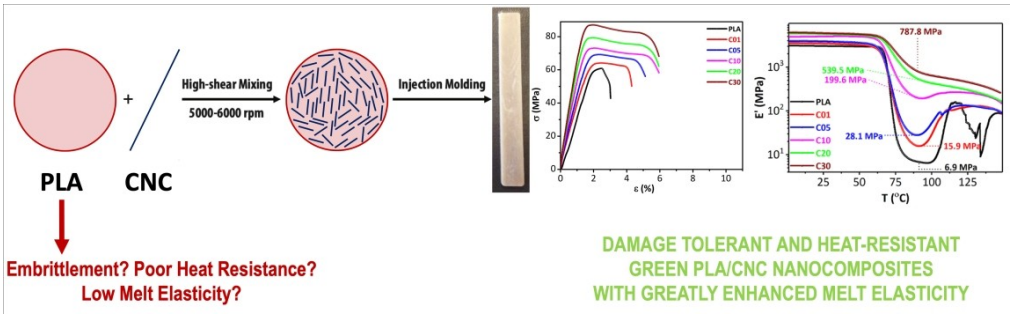

High-shear mixing with CNC leads to significant improvements in the toughness, heat resistance and melt elasticity of PLA while further enhancing its already outstanding room temperature stiffness and strength.

83x25mm (1200 x 1200 DPI)